



Macrophage-derived extracellular vesicles regulate concanavalin A-induced hepatitis by suppressing macrophage cytokine production

Reo Kawata^{a,b,*}, Shingo Oda^a, Yoshihiro Koya^c, Hiroaki Kajiyama^d, Tsuyoshi Yokoi^a

^a Department of Drug Safety Sciences, Division of Clinical Pharmacology, Nagoya University Graduate School of Medicine, 65 Tsurumai-cho, Showa-ku, Nagoya 466-8550, Japan

^b Department of Investigative Toxicology, Nonclinical Research Center, Tokushima Research Institute, Otsuka Pharmaceutical Co., Ltd., 463-10 Kagasuno, Kawauchi-cho, Tokushima, Japan

^c Bell Research Center Obstetrics and Gynecology, Academic Research & Industrial-Academia Collaboration, Nagoya University Graduate School of Medicine, 65 Tsurumai-cho, Showa-ku, Nagoya 466-8550, Japan

^d Department of Obstetrics and Gynecology, Nagoya University Graduate School of Medicine, 65 Tsurumai-cho, Showa-ku, Nagoya 466-8550, Japan

ARTICLE INFO

Keywords:

Key Words
Immune-mediated hepatitis
Extracellular vesicles
microRNAs
Macrophages
Concanavalin A

ABSTRACT

Acute liver failure is a clinical syndrome of severe hepatic dysfunction. Immune cells play an important role in acute liver failure. In recent years, the immunoregulatory function of extracellular vesicles (EVs) has been reported; therefore, it is inferred that EVs play a role in immune-mediated hepatitis. In this study, we investigated the immunoregulatory function of EVs in concanavalin A (Con A)-induced hepatitis. The mouse model was prepared by a single intravenous administration of 15 mg/kg Con A, in which there was a significant increase in the serum EVs number. In an *in vitro* study, the number of secreted EVs was also significantly increased in Con A-treated RAW264.7 cells, a mouse macrophage cell line, but not in Hepa1-6 cells, a mouse hepatoma cell line. In an *in vitro* EVs treatment study, EVs from Con A-treated mouse serum and Con A-treated RAW264.7 cells suppressed inflammatory cytokine production in Con A-stimulated RAW264.7 cells. miRNA sequencing analysis showed that the expression of mmu-miR-122-5p and mmu-miR-148a-3p was commonly increased in these EVs and EVs-treated cells. The pathways enriched in the predicted miRNA target genes included inflammatory response pathways. The mRNA levels of the target genes in these pathways (mitogen-activated protein kinase, phosphoinositide 3-kinase/Akt and Rho/Rho-associated coiled-coil containing protein kinase pathways) were decreased in the EVs-treated cells. In an *in vivo* RNA interference study, the knockdown of liver RAB27A, an EVs secretion regulator, significantly exacerbated Con A-induced hepatitis. These data suggest that macrophage-derived EVs play an important role in Con A-induced hepatitis through immunoregulation.

1. Introduction

Extracellular vesicles (EVs) are small vesicles with a diameter of 50–200 nm that are secreted from cells (Taylor and Gercel-Taylor, 2013). EVs include various molecules, such as RNAs and proteins, and play an important role in multiple diseases by transporting the molecules between cells (Alexander et al., 2017; Momen-Heravi et al., 2015; Tominaga et al., 2015). Therefore, EVs have attracted attention as therapeutic targets and tools and biomarkers in disease.

Acute liver failure is a clinical syndrome of abrupt severe hepatic dysfunction and has an approximately 30% mortality rate. The main causes of acute liver failure in the USA are autoimmune hepatitis, drug toxicity, viral hepatitis and ischemia (Stravitz and Lee, 2019). Immune-

related cells are involved in the pathogenesis of this disease. In autoimmune hepatitis, standard treatment is immunosuppressive therapy; however, most immunosuppressive agents have toxic adverse effects (Yang et al., 2019).

In recent years, the immune regulatory function of various cell-derived EVs has been reported (Holman et al., 2019; McDonald et al., 2014; Shao et al., 2020); therefore, in the present study, we inferred that EVs play a role in immune-mediated liver injury. In fact, EVs regulate the development and progression of various liver diseases, such as hepatic ischemia-reperfusion injury (Yang et al., 2018), alcoholic liver injury (Momen-Heravi et al., 2015; Saha et al., 2016), hepatic fibrosis (Seo et al., 2016) and nonalcoholic steatohepatitis (Hirsova et al., 2016), through the immunoregulation.

* The corresponding author at: Department of Drug Safety Sciences, Division of Clinical Pharmacology, Nagoya University Graduate School of Medicine, 65 Tsurumai-cho, Showa-ku, Nagoya 466-8550, Japan.

E-mail address: kawata.reo@otsuka.jp (R. Kawata).

<https://doi.org/10.1016/j.tox.2020.152544>

Received 14 May 2020; Received in revised form 21 July 2020; Accepted 27 July 2020

Available online 30 July 2020

0300-483X/ © 2020 Elsevier B.V. All rights reserved.

MicroRNAs (miRNAs) are small noncoding RNAs that are approximately 22 nucleotides in length. They are contained in EVs or bound to RNA-binding proteins and high-density lipoproteins in body fluids. miRNAs regulate gene expression through base-pairing with complementary sequences within target mRNAs (Harrill et al., 2016; Lawrie et al., 2008). miRNAs in EVs are transported between cells and regulate recipient cell function, such as the immune response, through gene expression regulation (Saha et al., 2016; Shao et al., 2020; Zhao et al., 2020).

In this study, we investigated the immunoregulatory function of EVs in immune-mediated hepatitis. Hepatitis was induced by the administration of concanavalin A (Con A), a lectin derived from jack beans, in mice. This model is widely used as a relevant model of human autoimmune hepatitis. In Con A-induced hepatitis, macrophages and T cells infiltrate the liver and play an important role in the development of hepatocellular apoptosis and necrosis through inflammatory cytokine, such as interleukin-6 (IL-6), interleukin-1 β (IL-1 β), tumor necrosis factor- α (TNF- α) and interferon- γ (IFN- γ), production (Xue et al., 2015). We investigated the effect of EVs from the model mouse serum or mouse cell lines on inflammatory cytokine production in macrophages. In addition, miRNA fluctuations in EVs and EVs-treated cells were analyzed to identify immunoregulatory molecules.

2. Materials and methods

2.1. Chemicals and reagents

Con A was purchased from Sigma-Aldrich (St. Louis, MO). Protease inhibitor cocktail set III DMSO solution ethylenediaminetetraacetic acid (EDTA) free was purchased from Fujifilm Wako Pure Chemical Corporation. The anti-CD63 antibody was purchased from System Biosciences (Palo Alto, CA), the anti-RAB27A antibody was purchased from Abcam (Cambridge, UK), the anti-GAPDH antibody was purchased from Novus Biologicals (Centennial, CO), and the IRDye 680 L T goat anti-rabbit IgG and IRDye 680 L T goat anti-mouse IgG antibodies were purchased from Li-Cor Biosciences (Lincoln, NE). All primers were synthesized at Hokkaido System Sciences (Sapporo, Japan). *Arabidopsis thaliana* (ath)-miR159a-3p was purchased from Hokkaido System Sciences. The adenovirus vector (AdV) *mRab27a* shRNA and AdV scrambled shRNA were obtained from Vector Biolabs (Malvern, PA).

2.2. Animals

Female BALB/c mice (7-8 weeks old) were obtained from Japan SLC (Hamamatsu, Japan). The animals were housed under a 12-h light/dark cycle in a controlled environment (maintained at 23 ± 2 °C with a relative humidity of $55 \pm 10\%$) in the institutional animal facility with *ad libitum* access to food and water; the mice were acclimated to our facility before the experiments were performed. All procedures performed on the animals were approved by the Animal Care Committee of Nagoya University Graduate School of Medicine and were carried out in accordance with the guidelines established by the Institute for Laboratory Animal Research of the Medical School of Nagoya University, Japan.

2.3. Mouse Con A treatment and sampling

For hepatitis induction, mice (8-9 weeks old) were intravenously administered a single dose of 15 mg/kg Con A dissolved in saline (5 mL/kg) as previously reported (Liu et al., 2015; Zheng et al., 2016). Blood samples were obtained from the caudal vena cava, and then the liver was collected under isoflurane anesthesia at 3, 6 or 9 h after the administration of Con A. The liver sample was fixed in 10% neutral buffered formalin for histopathological examination, or frozen in liquid nitrogen for RNA extraction and protein lysate preparation. The blood was clotted at room temperature and centrifuged at 1,600 g at 4 °C for

10 min to obtain serum. For EVs isolation, the obtained serum was centrifuged at 16,500 g at 4 °C for 20 min, and the supernatant (pretreated serum) was stored at -80 °C until use.

2.4. Histopathological examination

The fixed livers were dehydrated with a graded series of ethyl alcohol, dealcoholized with xylene, and embedded in paraffin. These samples in paraffin blocks were thinly sectioned and stained with hematoxylin and eosin (H&E). The specimens were examined by light microscopy.

2.5. Serum biochemical analysis

The level of serum alanine transaminase (ALT) was measured using a Dri-Chem 4000 system (Fujifilm, Tokyo, Japan).

2.6. EVs isolation from the serum

The pretreated serum was centrifuged at 208,000 g at 4 °C for 70 min using an MLS-50 rotor (Beckman Coulter, Brea, CA). The EVs pellets were washed once with phosphate-buffered saline (PBS) filtered through a 0.22 μ m filter (Corning, Corning, NY). And then, the following reagents were added to the pellet: PBS filtered through a 0.22 μ m filter for NanoSight assays, RIPA buffer containing 1% Nonidet P-40, 0.1% sodium dodecyl sulfate (SDS), 50 mM Tris-HCl buffer (pH 8.0), 150 mM NaCl, 5 mM EDTA, 50 mM sodium fluoride, 1 mM sodium orthovanadate (Na₃VO₄), 25 mM disodium β -glycerophosphate pentahydrate and a protease inhibitor cocktail for the Western blot assays or QIAzol Lysis Reagent (Qiagen, Valencia, CA) for RNA extraction.

2.7. Analysis of EVs size and concentration

The EVs suspended in PBS were measured using a NanoSight NS300 system (Malvern Panalytical, Malvern, Worcs, UK).

2.8. Western blot assay

SDS-polyacrylamide gel electrophoresis and immunoblot analysis were performed according to the method described by Laemmli (Laemmli, 1970). The homogenized liver samples or EVs samples with RIPA buffer were used as protein lysates. The lysates were boiled for 3 min with SDS and 2-mercaptoethanol to be resolved. The resolved samples were separated on a 10% SDS-polyacrylamide gel and electrotransferred onto an Immobilon-P membrane (Millipore Corporation, Billerica, MA). The membrane was blocked in Odyssey blocking buffer (Li-Cor Biosciences) and incubated with anti-CD63, anti-RAB27A or anti-GAPDH antibodies at 4 °C overnight. Subsequently, the membrane was incubated with a fluorescent dye-conjugated secondary antibody for 1 h. The fluorescence signal was detected using the Odyssey Infrared Imaging System (Li-Cor Biosciences).

2.9. Cell culture

The mouse macrophage RAW264.7 cell line was obtained from RIKEN BioResource Research Center (Ibaraki, Japan). The mouse hepatoma Hepa1-6 cell line was kindly provided by Dr. S. Kaneko (Kanazawa University, Japan) (Marukawa et al., 2012). HEK293 cells were obtained from the American Type Culture Collection (Manassas, VA). The cells were maintained in Dulbecco's modified Eagle's medium (Nissui Pharmaceutical, Tokyo, Japan) supplemented with 10% fetal bovine serum (Sigma-Aldrich), 2 mM glutamine and 3.5 g/L glucose (Fujifilm Wako Pure Chemical Corporation) at 37 °C in a 5% CO₂ atmosphere.

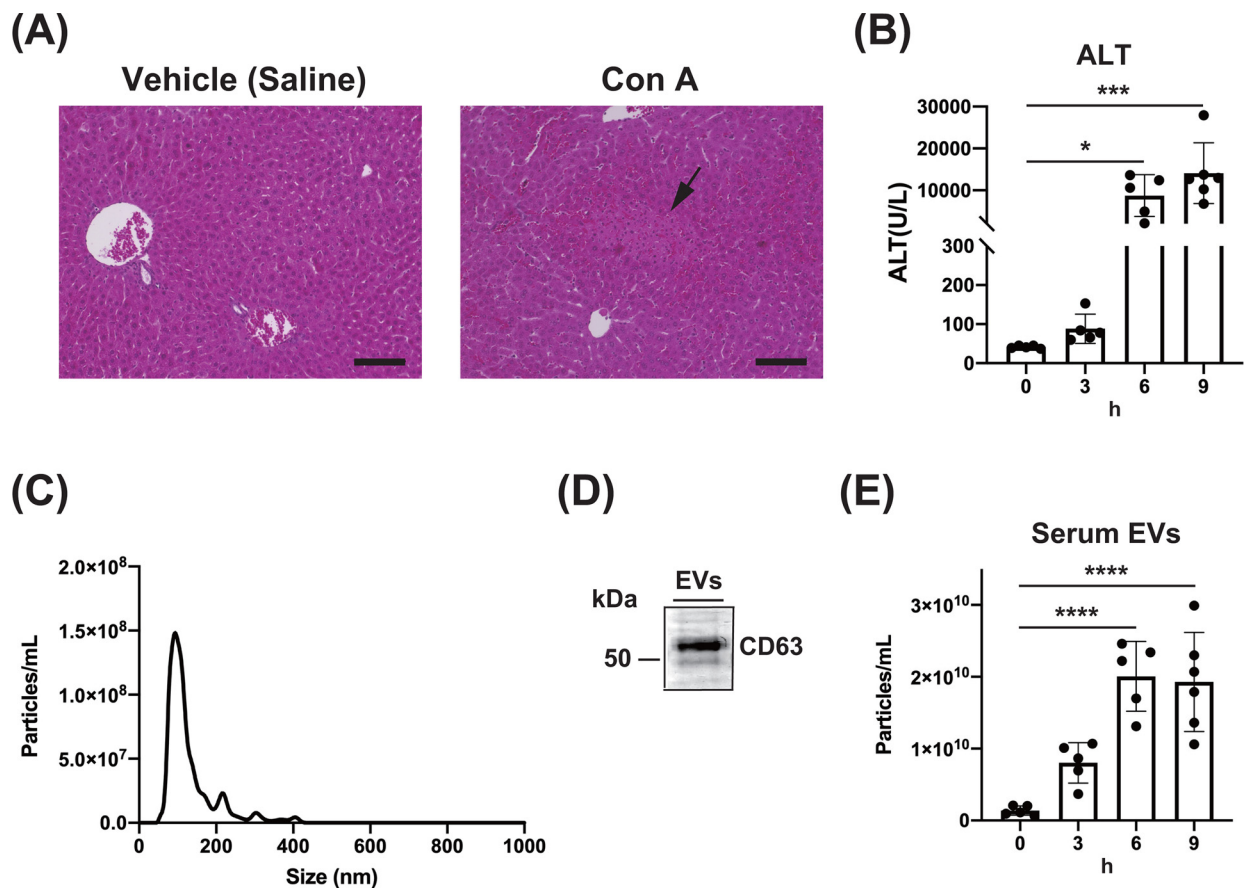


Fig. 1. Histopathological examination of the livers and changes in the serum ALT levels and serum EVs numbers in the Con A-administered mice.

Representative image of H&E-stained liver sections from Con A (15 mg/kg)-administered mice at 9 h is shown (A). The black arrow shows the massive necrosis of hepatocytes. Scale bar = 100 μ m. The serum ALT levels in the Con A-administered mice at 0, 3, 6 and 9 h are shown (B). Representative particle plot data of saline-treated mouse serum EVs is shown (C). CD63 expression in saline-treated mouse serum EVs was analyzed by Western blotting, and representative data is shown (D). The serum EVs numbers in the Con A-administered mice at 0, 3, 6 and 9 h are shown (E). The data are shown as the mean value \pm S.D. (n = 5-6/group). Differences in the posttreatment values compared with the pretreatment values were considered significant at *p < 0.05, ***p < 0.001 and ****p < 0.0001.

2.10. Con A cytotoxicity in RAW264.7 and Hepa1-6 cells

RAW264.7 and Hepa1-6 cells were seeded at a density of 3×10^4 and 1.5×10^4 cells/well, respectively, and preincubated for 24 h. After 24 h of incubation with Con A or vehicle (1% saline in the culture medium), the cellular adenosine triphosphate (ATP) levels were measured using a CellTiter-Glo 2.0 Cell Viability Assay (Promega, Madison, WI) and a microplate reader (Infinite 200 PRO, Tecan Group Ltd., Männedorf, Switzerland) according to the manufacturer's protocol.

2.11. EVs isolation from Con A-treated RAW264.7 and Hepa1-6 cell culture supernatants

EVs in FBS were removed by centrifugation at 175,000 g at 4 $^{\circ}$ C for 16 h using an SW32Ti rotor (Beckman Coulter), and EVs-free culture medium was prepared with the EVs-free FBS. RAW264.7 and Hepa1-6 cells were seeded at a density of 3×10^6 and 1.5×10^6 cells/plate, respectively, and preincubated for 24 h. After cells were incubated for 24 h with Con A or vehicle in EVs-free culture medium, the culture supernatants were collected and centrifuged at 2,000 g at 4 $^{\circ}$ C for 10 min. The supernatants were filtered through a 0.2 μ m syringe filter (Sartorius, Göttingen, Germany) and then centrifuged at 175,000 g at 4 $^{\circ}$ C for 4 h using an SW32Ti rotor. The EVs pellets were washed once with PBS filtered through a 0.22 μ m filter. And then, the following reagents were added to the pellet: PBS filtered through a 0.22 μ m filter, RIPA buffer with a protease inhibitor cocktail or QIAzol Lysis Reagent.

2.12. Con A treatment of RAW264.7 cells for total RNA extraction

RAW264.7 cells were seeded at a density of 1.5×10^5 cells/well and preincubated for 24 h. After being incubated for 24 h with Con A or vehicle, the cells were harvested for RNA extraction.

2.13. in vitro cellular uptake of EVs

The serum EVs or RAW264.7-derived EVs suspended in PBS were fluorescently labeled using an ExoSparkler Exosome Membrane Labeling kit (Dojindo, Kumamoto, Japan) according to the manufacturer's protocols. RAW264.7 cells were seeded at a density of 1.5×10^5 cells/well in 24-well glass-bottom plates and preincubated for 24 h. After being incubated for 8 h with 6E + 09 labeled EVs/mL in EVs-free medium, the cells were stained with 4',6'-diamidino-2-phenylindole dihydrochloride (DAPI) for nuclear staining and observed by fluorescence microscopy (BZ-9000, KEYENCE, Osaka, Japan).

2.14. Cell viability of EVs-treated RAW264.7 cells

RAW264.7 cells were seeded at a density of 3×10^4 cells/well and preincubated for 24 h. After being incubated for 24 h with 6E + 09 EVs/mL in EVs-free medium, the cell viability was evaluated using Cell Counting Kit-8 (Dojindo) according to the manufacturer's protocols.

EVs and Con A cotreatment of RAW264.7 cells for RNA extraction and the measurement of culture supernatant IL-6 levels

RAW264.7 cells were seeded at a density of 1.5×10^5 cells/well

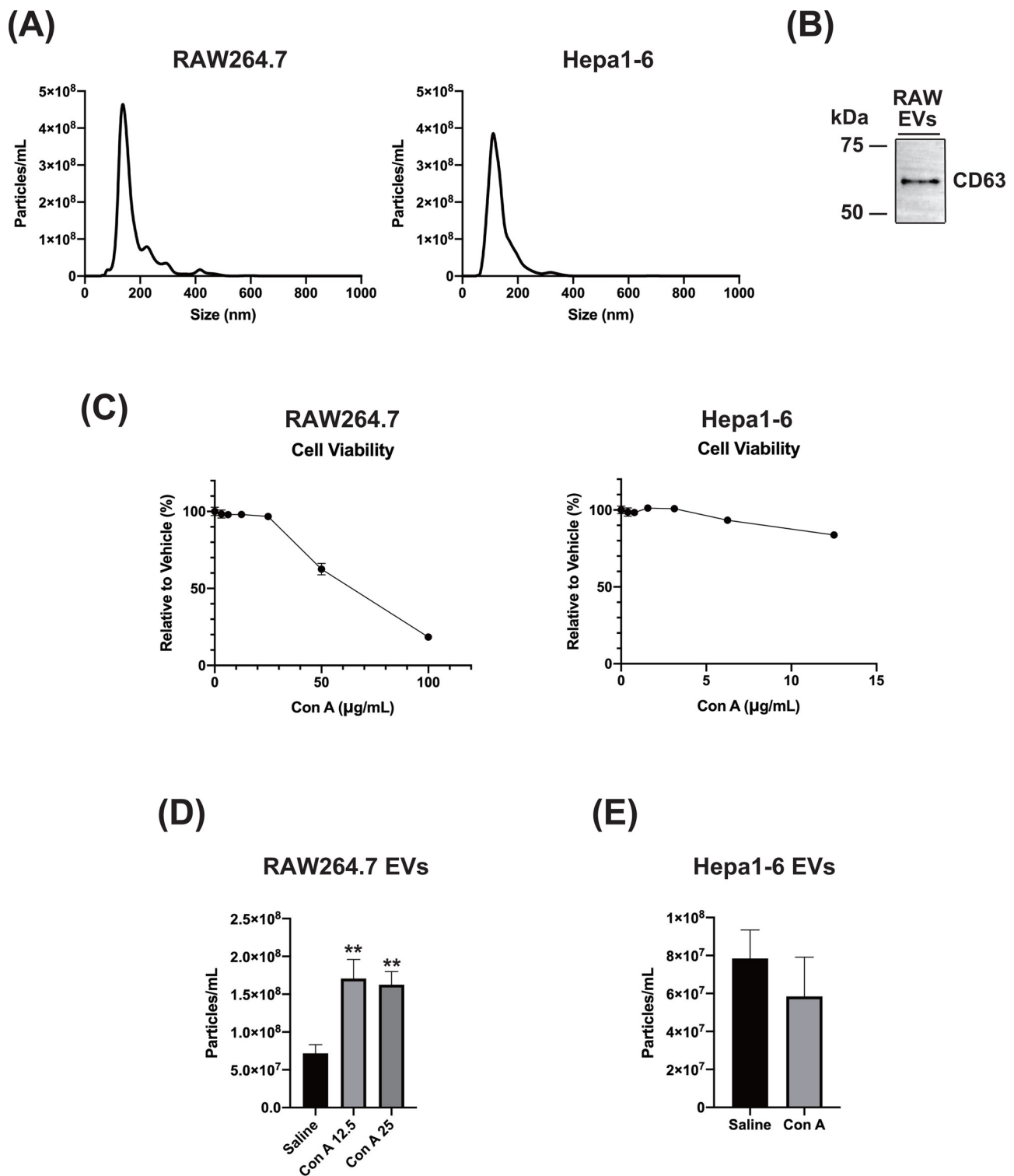
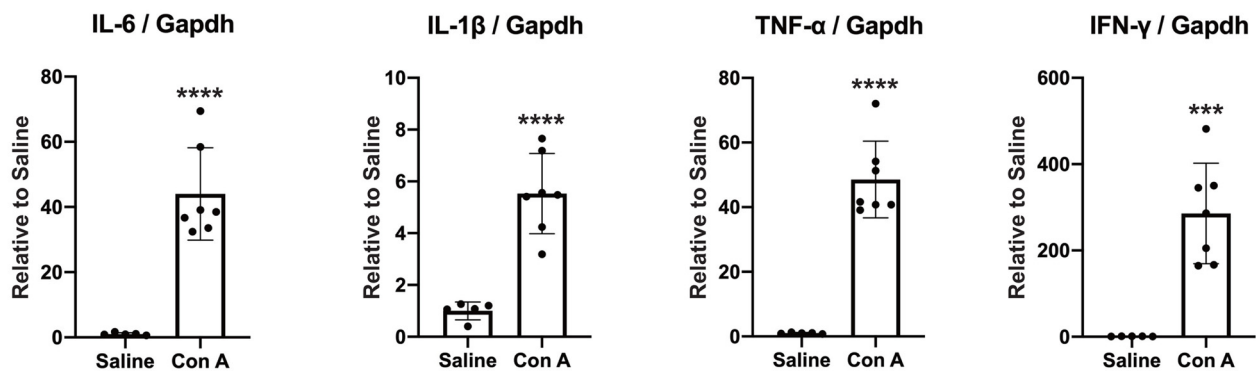


Fig. 2. Cell viability and secreted EVs numbers in Con A-treated RAW264.7 cells and Hepa1-6 cells. Representative particle plot data of the secreted EVs from the saline-treated RAW264.7 cells and Hepa1-6 cells are shown (A). CD63 expression in the secreted EVs from the saline-treated RAW264.7 cells was analyzed by Western blotting, and representative data is shown (B). The viability of the RAW264.7 cells treated with 0, 3.13, 6.25, 12.5, 25, 50 or 100 µg/mL Con A for 24 h and the Hepa1-6 cells treated with 0, 0.39, 0.78, 1.56, 3.13, 6.25 or 12.5 µg/mL Con A for 24 h were evaluated by an intracellular ATP assay, and the data are shown as the mean value ± S.D. (n = 4/group) (C). The EVs numbers in the culture supernatants of the 12.5 or 25 µg/mL Con A-treated RAW264.7 cells (D) and 3.13 µg/mL Con A-treated Hepa1-6 cells (E) at 24 h are shown. The data are shown as the mean value ± S.D. (n = 3/group). Differences in the Con A-treated groups compared with the saline-treated group were considered significant at ****p < 0.01**.

and preincubated for 24 h. After being incubated for 8 h incubation with $6E + 09$ EVs/mL in EVs-free medium, the cells were treated with Con A or vehicle. After further incubation for 16 h, the cells and culture supernatants were harvested for RNA extraction and IL-6 level

measurement, respectively. IL-6 levels were measured using a mouse IL-6 Quantikine ELISA kit (R&D Systems Inc., Minneapolis, MN) and a microplate reader (Infinite 200 PRO) according to the manufacturer's protocols.

(A)



(B)

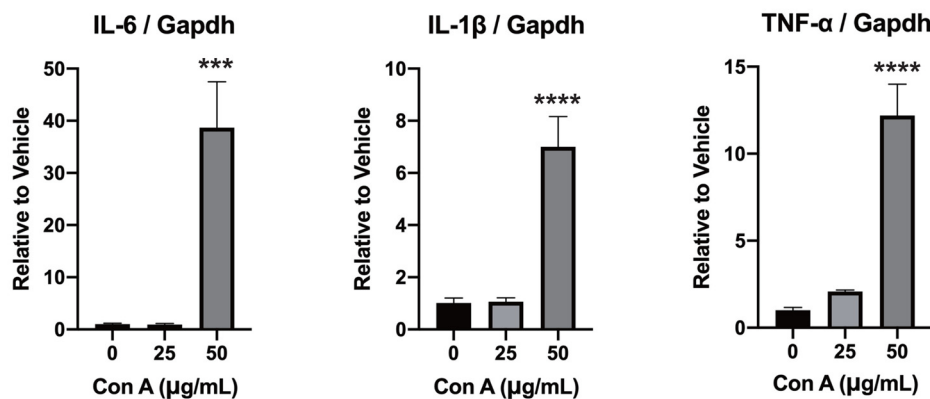


Fig. 3. Induction of inflammatory cytokine expression in the livers of Con A-treated mice and Con A-treated RAW264.7 cells.

IL-6, IL-1 β , TNF- α and IFN- γ mRNA levels in the livers of the Con A-administered mice at 9 h were analyzed by qPCR (n = 5-7/group) (A). IL-6, IL-1 β and TNF- α mRNA levels in the RAW264.7 cells treated with 0, 25 or 50 μ g/mL Con A for 24 h were analyzed by qPCR (n = 3/group) (B). The mRNA levels were normalized to those of *Gapdh*. The data are shown as the mean value \pm S.D. Differences in the Con A-treated group compared with the saline-treated group were considered significant at ***p < 0.001 and ****p < 0.0001.

2.15. Real-time reverse transcription-polymerase chain reaction (RT-PCR)

For RT-PCR, total RNA of mouse liver and RAW264.7 cells was extracted using RNAiso Plus (TAKARA Bio, Shiga, Japan) and TRIzol Reagent (Thermo Fisher Scientific, Waltham, MA), respectively, according to the manufacturer's protocols. The mRNA levels of IL-6, IL-1 β , TNF- α , IFN- γ , mitogen-activated protein kinase kinase 1 (*Map2k1*), mitogen-activated protein kinase kinase kinase 13 (*Map3k13*), *Akt3*, Rho associated coiled-coil containing protein kinase 1 (*Rock1*) or glyceraldehyde-3-phosphate dehydrogenase (*Gapdh*) were quantified by real-time RT-PCR. Reverse transcription was performed using a ReverTra Ace qPCR RT kit (Toyobo, Osaka, Japan), and real-time RT-PCR was performed using SYBR Premix Ex Taq (Tli RNaseH Plus) (TAKARA Bio) according to the manufacturer's protocol. The RNA concentration was quantified using a NanoDrop (Thermo Fisher Scientific), and 1 μ g of RNA was used for reverse transcription. The following PCR thermal cycle was used: denaturation at 95 $^{\circ}$ C for 30 s, followed by 40 amplification cycles of 95 $^{\circ}$ C for 5 s and 60 $^{\circ}$ C for 30 s using an Mx3000p (Agilent Technologies, Santa Clara, CA). The primer sequences used in this study are shown in Table S1.

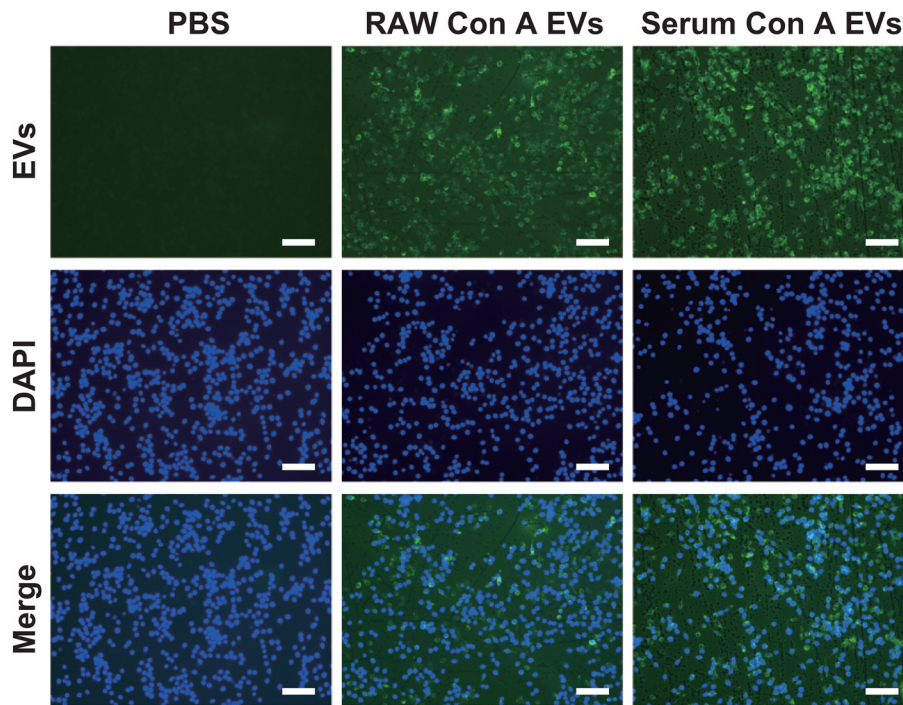
2.16. cDNA library synthesis and miRNA sequencing (miRNA-seq)

Total RNA of RAW264.7 cells was extracted using a miRNeasy Mini kit (Qiagen) according to the manufacturer's protocol. For EVs RNA extraction, ath-miR159a-3p, a spike-in control, was added to the EVs lysate in QIAzol Lysis Reagent, and total RNA was extracted using a miRNeasy Serum/Plasma kit (Qiagen) according to the manufacturer's protocol. The quantity and quality of the RNA samples were checked with an Agilent BioAnalyzer (Agilent Technologies, Santa Clara, CA) using an RNA6000 Pico Kit (Agilent Technologies). cDNA libraries for miRNA-seq were synthesized with an NEBNext Multiplex Small RNA Library Prep Set for Illumina (New England Biolabs Inc., Ipswich, MA) and quantified with a Qubit 2.0 fluorometer (Life Technologies, Carlsbad, CA) using a Qubit dsDNA HS Assay kit (Life Technologies) according to the manufacturer's protocol. miRNA-seq was performed with an Illumina MiSeq System using MiSeq Reagent Kit v3 (Illumina, San Diego, CA). For improved cluster formation, denatured Phix control v3 (Illumina) was added to the cDNA libraries. Sequencing was performed with 51 bp single-end reads.

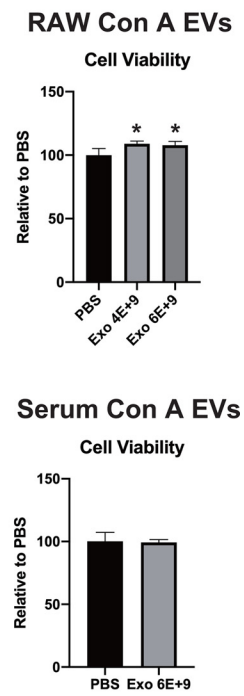
2.17. Differential expression analysis of the miRNA-seq count data

The FASTQ files generated by the Illumina MiSeq System were

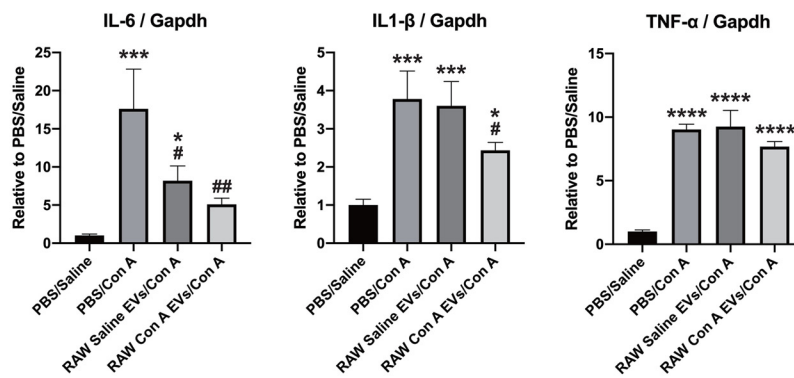
(A)



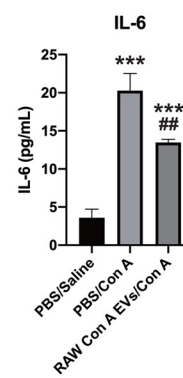
(B)



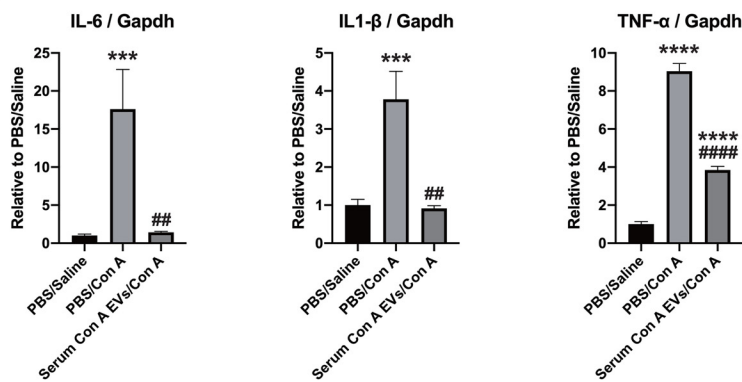
(C)



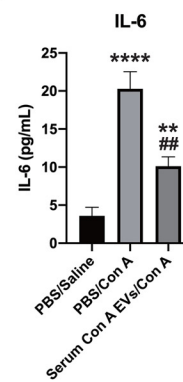
(D)



(E)



(F)



(caption on next page)

Fig. 4. Suppression of inflammatory cytokine production in Con A-stimulated RAW264.7 cells by EVs pretreatment.

RAW264.7 cells were treated with 6E + 09 particles/mL fluorescently labeled RAW Con A EVs or Serum Con A EVs for 8 h, and nuclei were stained with DAPI. Representative images obtained by fluorescence microscopy are shown (A). Scale bar = 100 μ m. RAW264.7 cells were treated with 4E + 09 or 6E + 09 particles/mL RAW Con A EVs or Serum Con A EVs for 24 h, and the cell viability was evaluated using Cell Counting Kit-8 ($n = 4$ /group) (B). RAW264.7 cells were pretreated with 6E + 09 EVs/mL for 8 h, followed by 50 μ g/mL Con A treatment for 16 h. *IL-6*, *IL-1 β* and *TNF- α* mRNA levels in the RAW Saline EVs/Con A-cotreated cells or RAW Con A EVs/Con A-cotreated cells (C) and IL-6 protein level in the culture supernatants of the cells (D) are shown ($n = 3$ /group). *IL-6*, *IL-1 β* and *TNF- α* mRNA levels in the Serum Con A EVs/Con A-cotreated cells (E) and IL-6 protein levels in the culture supernatants of the cells (F) are shown ($n = 3$ /group). “PBS/Saline” and “PBS/Con A” indicate PBS/Saline-cotreated cells and PBS/Con A-cotreated cells, respectively. The mRNA levels were normalized to those of *Gapdh*. The data are shown as the mean value \pm S.D. Differences in comparisons with each vehicle group were considered significant at * $p < 0.05$, ** $p < 0.01$, *** $p < 0.001$ and **** $p < 0.0001$. Differences in comparisons with the PBS/Con A-cotreated group were considered significant at # $p < 0.05$, ## $p < 0.01$ and ### $p < 0.0001$.

analyzed with CLC Genomics Workbench (Qiagen). Adaptor sequences were trimmed, and sequences with a length less than 15 or greater than 35 bp were discarded before counting. The trimmed data were mapped to the mouse mature miRNA sequence in miRbase ver. 22.1, allowing two-base mismatches. In the EVs miRNA analysis, the trimmed data were also mapped to mature ath-miRNA sequences with perfect matches. miRNAs with a total sample read count less than 10 were filtered out. In the RAW264.7 miRNA analysis, normalization and statistical analysis were performed by the edgeR package using TCC-GUI (Su et al., 2019) and the differentially expressed miRNA genes (DEGs) were identified in the comparison with each control group using a q value < 0.1 and fold change > 2 or < 0.5 . In the EVs miRNA analysis, the read counts were normalized by dividing by the read counts of the spike-in control miRNA, and DEGs were identified in comparisons with each control group using a fold change > 2 or < 0.5 . A set of FASTQ files and raw and normalized read count data are available in the NCBI Gene Expression Omnibus (GEO; accession: GSE147243). Hierarchical clustering was performed using Spearman's correlation as a distance and complete linkage as a linkage criterion, and a heatmap was generated for the z-scores of normalized read counts using genefilter and gplots packages with R software (ver. 3.4.0). MA plots were generated for the normalized read counts using the ggplot2 package. Venn diagrams were generated using Venn Draw software (ver. 0.2).

2.18. Prediction of miRNA target genes and pathway enrichment analysis

The prediction of mmu-miR-122-5p and mmu-miR-148a-3p target genes was performed by miRWalk2.0 (Dweep and Gretz, 2015). The 10 algorithms in miRWalk2.0 (miRWalk, MicroT4, miRanda, miRDB, miRMap, miRNAMap, PITA, RNA22, RNAhybrid and TargetsScan) were used, and the 3'UTR was applied as the target site for the prediction. The genes that produced hits in more than 8 algorithms were identified as predicted target genes. KEGG pathway enrichment analysis of the predicted target genes was performed by DAVID version 6.8 (Huang et al., 2009). The enriched pathways were identified with a p value < 0.05 . The validated target genes of mmu-miR-122-5p and mmu-miR-148a-3p were searched using miRTarbase (Huang et al., 2020).

2.19. Propagation and purification of adenoviral vectors

AdV *mRab27a* shRNA and AdV scrambled shRNA were propagated in HEK293 cells. The AdVs were purified by cesium chloride-gradient ultracentrifugation according to the method described by Ugai et al. (Ugai et al., 2005). Viral titers were determined by the Adeno-XTM Rapid Titer kit (TAKARA Bio) according to the manufacturer's protocol. The cells were infected with AdVs in culture medium containing 5% FBS.

2.20. AdV and Con A treatment of mice and sampling

Three days after a single intravenous administration of AdV *mRab27a* shRNA or AdV scrambled shRNA at 1E + 10 ifu/mouse diluted in PBS, the mice were intravenously administered a single dose of 15 mg/kg Con A dissolved in saline. Blood and liver samples were

collected 9 h after the administration of Con A.

2.21. Statistical analysis

All values are presented as the mean \pm standard deviation (S.D.). Statistical analysis was performed using GraphPad Prism software (GraphPad Software, San Diego, CA). Comparisons of multiple groups were performed using one-way ANOVA with Dunnett's post hoc test. Comparisons of two groups were performed using Student's t test.

3. Results

3.1. Significant increase in numbers of serum EVs in the Con A-induced hepatitis model mice

To evaluate hepatitis in Con A-treated mice, histopathological changes were examined, and serum ALT levels were measured. Massive necrosis of hepatocytes (black arrow) was observed in the livers 9 h after Con A (15 mg/kg) administration (Fig. 1A), and compared with the preadministration serum ALT values, those observed 6 and 9 h after Con A administration were significantly increased (Fig. 1B).

To examine the change in serum EVs numbers in this model, EVs were isolated by ultracentrifugation. The EVs were particles with mean diameters of approximately 100 nm (Fig. 1C). The CD63 signal, an EVs marker, was detected in the serum EVs sample by Western blotting (Fig. 1D). Compared with the preadministration numbers, the serum EVs numbers increased significantly in a time-dependent manner after Con A administration (Fig. 1E).

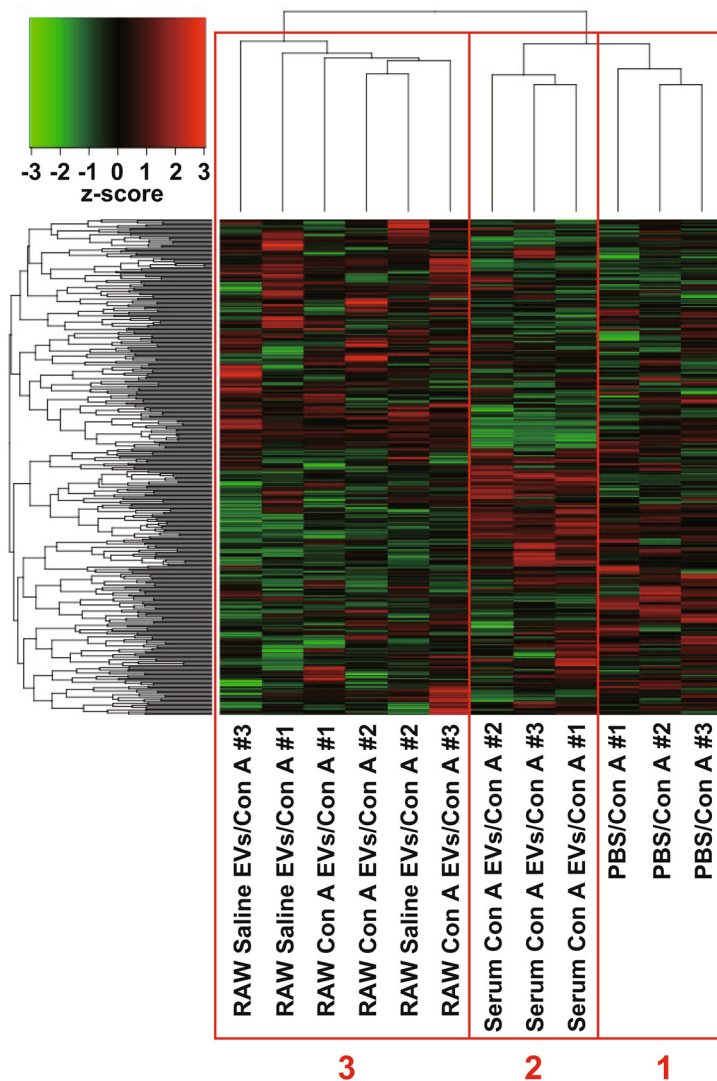
3.2. Induction of EVs secretion in RAW264.7 cells but not Hepa1-6 cells by Con A treatment

To clarify from which cells the increased serum EVs were derived in the Con A-treated mice, the numbers of secreted EVs from Con A-treated mouse cell lines were examined. The EVs isolated from the culture supernatant of RAW264.7 cells, a mouse macrophage cell line, and Hepa1-6 cells, a mouse hepatoma cell line, had mean diameters of approximately 100 nm (Fig. 2A). The CD63 signal was detected in the EVs from RAW264.7 cells by Western blot (Fig. 2B).

To determine the Con A dose for the induction of EVs secretion, the Con A cytotoxicity in RAW264.7 cells and Hepa1-6 cells was examined by intracellular ATP assay. Intracellular ATP concentrations greater than 95% of the vehicle-treated cells were produced in ≤ 25 μ g/mL Con A-treated RAW264.7 cells and in ≤ 3.13 μ g/mL Con A-treated Hepa1-6 cells (Fig. 2C). Therefore, 12.5 and 25 μ g/mL Con A for RAW264.7 cells and 3.13 μ g/mL Con A for Hepa1-6 cells were adopted for subsequent experiments.

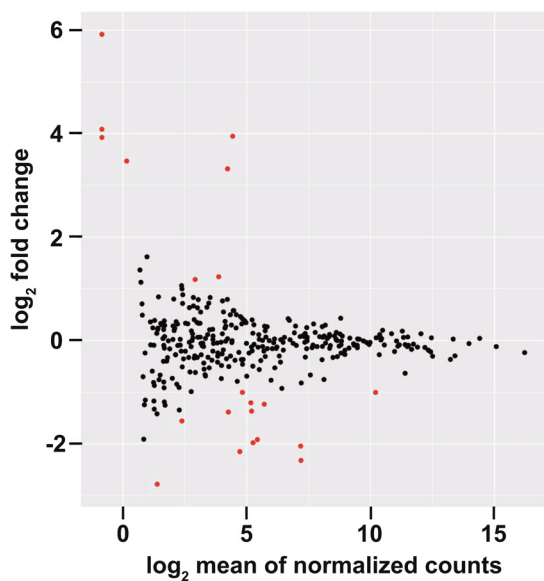
Compared with those from the saline-treated cells, the numbers of secreted EVs from the RAW264.7 cells treated with 12.5 or 25 μ g/mL Con A for 24 h were significantly increased (Fig. 2D). However, there was no change in the number of EVs secreted from Con A-treated Hepa1-6 cells (Fig. 2E). These data suggest that the increased serum EVs in the Con A-treated mice are derived from macrophages rather than hepatocytes.

(A)

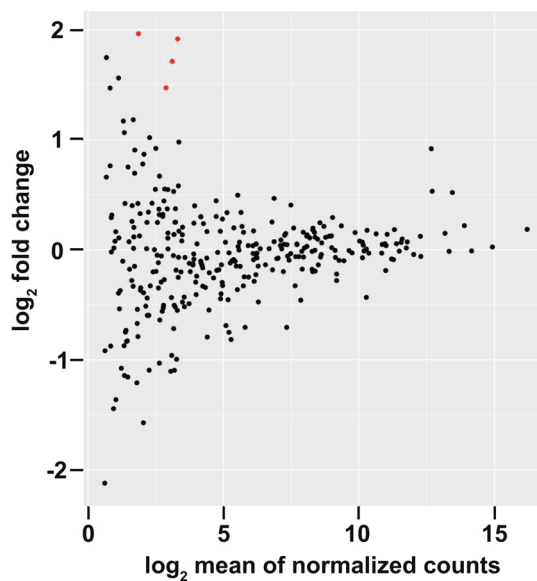


(B)

Serum Con A EVs/Con A vs PBS/Con A



RAW Con A EVs/Con A vs PBS/Con A



(caption on next page)

Fig. 5. miRNA profiling in the EVs/Con A-cotreated RAW264.7 cells by miRNA-seq analysis.

RAW264.7 cells were pretreated with $6E + 09$ EVs/mL for 8 h, followed by 50 μ g/mL Con A treatment for 16 h. Total RNA was extracted from the cells, and miRNA-seq analysis was performed ($n = 3$ /group). PBS/Con A, RAW Saline EVs/Con A, RAW Con A EVs/Con A and Serum Con A EVs/Con A indicate each cotreated cells. Hierarchical clustering was performed using Spearman's correlation as a distance and complete linkage as a linkage criterion; a heatmap was generated for the z-scores of the normalized read counts of miRNAs (A). Differentially expressed miRNA genes (DEGs) compared with those in the PBS/Con A group were identified with a q value < 0.1 and fold change > 2 or < 0.5 . MA plots for normalized read counts of miRNAs in Serum Con A EVs/Con A vs PBS/Con A (B, left panel) and RAW Con A EVs/Con A vs PBS/Con A (B, right panel) show the DEGs and the non-DEGs with red dots and black dots, respectively.

3.3. Con A treatment-induced inflammatory cytokine production in the liver and RAW264.7 cells

To examine the involvement of inflammatory cytokines in Con A-induced hepatitis, the hepatic inflammatory cytokine levels in the hepatitis model mice were measured by qPCR. Significant increases in hepatic *IL-6*, *IL-1 β* , *TNF- α* and *IFN- γ* levels were observed in the 9 h Con A administration group compared with the vehicle group (Fig. 3A). Next, we examined whether the inflammatory cytokine production is enhanced in Con A-stimulated macrophages-derived cells. Significant increases in *IL-6*, *IL-1 β* and *TNF- α* levels were observed in the 50 μ g/mL Con A-treated RAW264.7 cells compared with the vehicle-treated cells (Fig. 3B). A PCR amplification product for *IFN- γ* could not be detected in RAW264.7 cells under the current assay conditions. These data suggest that the inflammatory cytokine production in hepatic macrophage cells is enhanced in Con A-induced hepatitis.

3.4. Suppression of inflammatory cytokine production in RAW264.7 cells treated with EVs

We examined the effect of EVs on inflammatory cytokine production in RAW264.7 cells. To examine whether the isolated EVs could be incorporated into RAW264.7 cells, RAW264.7 cells were treated with the fluorescently labeled RAW Con A EVs (EVs from Con A-treated RAW264.7 cells) or Serum Con A EVs (serum EVs from Con A-treated mice). The uptake of both EVs types into cells was observed (Fig. 4A). The RAW264.7 cell viability was not reduced by these EVs treatments (Fig. 4B). To examine the effect of EVs on inflammatory cytokine production in Con A-stimulated RAW264.7 cells, cells were pretreated with EVs prior to Con A treatment, and inflammatory cytokine expression was analyzed. *IL-6* mRNA levels were significantly suppressed in RAW Saline EVs (EVs from saline-treated RAW264.7 cells)/Con A-cotreated cells, and *IL-6* and *IL-1 β* mRNA levels were significantly suppressed in RAW Con A EVs/Con A-cotreated cells (Fig. 4C). The *IL-6* protein level in the culture supernatant was also significantly suppressed in RAW Con A EVs/Con A-cotreated cells (Fig. 4D). In Serum Con A EVs/Con A-cotreated cells, *IL-6*, *IL-1 β* and *TNF- α* mRNA levels (Fig. 4E) and the *IL-6* protein level in the culture supernatant (Fig. 4F) were significantly suppressed.

3.5. miRNA profiling in EVs-treated RAW264.7 cells and EVs

To search for immunosuppressive factors in EVs, miRNA-seq of EVs/Con A-cotreated RAW264.7 cells was performed ($n = 3$ /group). The RNA integrity numbers in all RAW264.7 RNA samples were greater than 8 (data not shown). The cluster analysis identified three clusters: 1. PBS/Con A-cotreated group, 2. Serum Con A EVs/Con A-cotreated group, and 3. RAW Saline EVs/Con A-cotreated group and RAW Con A EVs/Con A-cotreated group (Fig. 5A). In Serum Con A EVs/Con A-cotreated cells, the expression of 8 miRNAs was significantly increased (q value < 0.1 , fold change > 2) and the expression of 13 miRNAs was significantly decreased (q value < 0.1 , fold change < 0.5) compared with that in PBS/Con A-cotreated cells (Fig. 5B left panel and Table S2). In RAW Con A EVs/Con A-cotreated cells, the expression of 4 miRNAs was significantly increased (q value < 0.1 , fold change > 2) compared with that in PBS/Con A-cotreated cells (Fig. 5B right panel and Table S3).

miRNA-seq in the EVs from serum or RAW264.7 cells was also performed ($n = 1$ /group). For the EVs miRNA analysis, the normalized read counts divided by the read counts of the spike-in control miRNA were used. In Serum Con A EVs, the expression of 273 miRNAs was increased (fold change > 2) and the expression of 1 miRNA was decreased (fold change < 0.5) compared with that in Serum Saline EVs (serum EVs from saline-treated mice) (the top 35 increased miRNAs are shown in Table S4). In RAW Con A EVs, the expression of 79 miRNAs was increased (fold change > 2), and the expression of 97 miRNAs was decreased (fold change < 0.5) compared with that in RAW Saline EVs (the top 35 increased miRNAs are shown in Table S5).

To identify the miRNAs transported into RAW264.7 cells by macrophage-derived EVs, we extracted the common miRNAs with increased expression. In the RAW264.7 miRNAs, there were 2 miRNAs commonly increased in Serum Con A EVs/Con A-cotreated cells and RAW Con A EVs/Con A-cotreated cells (Fig. 6A upper left panel). In the EVs miRNAs, 49 miRNAs were commonly increased in Serum Con A EVs and RAW Con A EVs (Fig. 6A upper right panel). Then, there were 2 common miRNAs (*mmu-miR-122-5p* and *mmu-miR-148a-3p*) in the commonly increased miRNAs in RAW264.7 cells and EVs (Fig. 6A lower panel). The normalized read counts of *mmu-miR-122-5p* and *mmu-miR-148a-3p* in the Serum Con A EVs/Con A-cotreated RAW264.7 cells, RAW Con A EVs/Con A-cotreated cells, Serum EVs and RAW EVs are shown in Figs. 6B, 6C, 6D and 6E, respectively. These miRNAs were more abundant in Serum Con A EVs/Con A-cotreated RAW264.7 cells than in RAW Con A EVs/Con A-cotreated cells (Figs. 6B and 6C). These data suggest that the two miRNAs may be transported into RAW264.7 cells by macrophage-derived EVs and involved in the immunoregulation observed in the EVs-treated cells (Figs. 4C-4 F).

3.6. Suppression of *mmu-miR-122-5p* and *mmu-148a-3p* target gene expression in RAW264.7 cells by EVs treatment

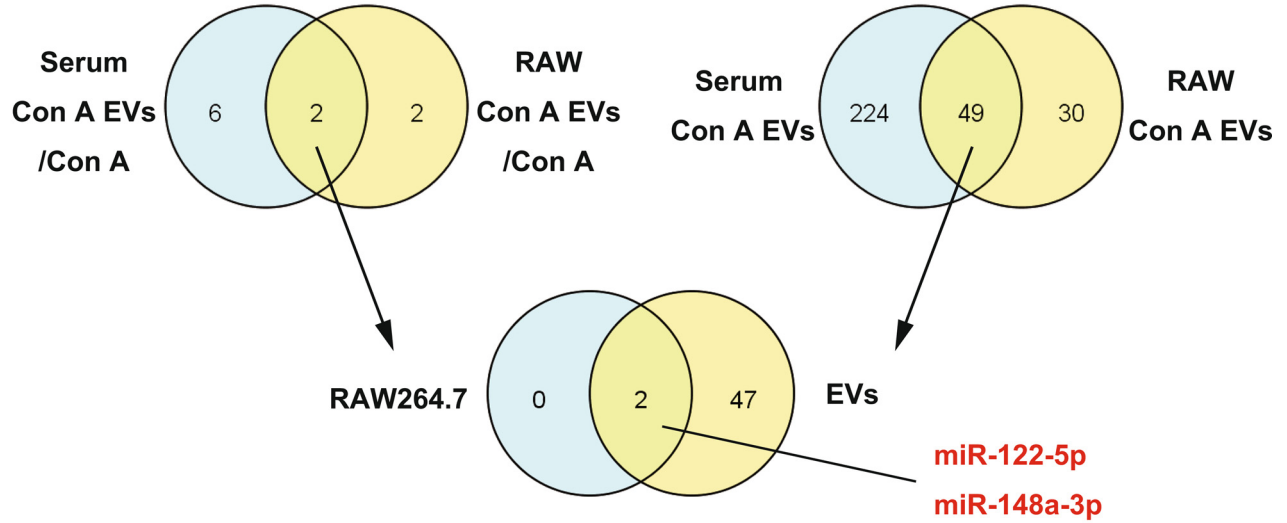
The prediction analysis of *mmu-miR-122-5p* and *mmu-miR-148a-3p* target genes by miRWalk2.0 identified 592 and 843 genes, respectively (data not shown). Thereafter, a KEGG pathway enrichment analysis of the predicted target genes was performed by DAVID. The enriched pathways (p value < 0.05) included the pathways involved in an inflammatory response (Table 1).

Among the predicted target genes, the gene expression levels in the mitogen-activated protein kinase (MAPK) signaling pathway and phosphatidylinositol-3 kinase (PI3K)/Akt signaling pathway, which regulate the production of inflammatory cytokines, such as *IL-6* (Deng et al., 2019; Hou et al., 2018; Li et al., 2019), were analyzed in the EVs/Con A-cotreated RAW264.7 cells. *Map2k1*, *Map3k13* and *Akt3* mRNA levels were significantly decreased or tended to decrease in response to EVs pretreatment (Figs. 7A and 7B). In addition, we searched the validated target genes of *mmu-miR-122-5p* and *mmu-miR-148a-3p* using miRTarbase. Among the validated target genes, qPCR was performed on *Rock1* gene related in the Rho/ROCK pathway, which regulates the production of inflammatory cytokines, such as *IL-6* (Cheng et al., 2015; Gong et al., 2018). *Rock1* mRNA levels were significantly decreased by EVs pretreatment (Fig. 7C). A list of the genes analyzed by qPCR is shown in Table 2.

(A)

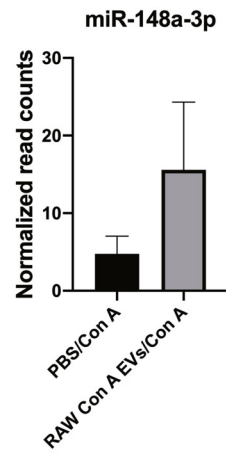
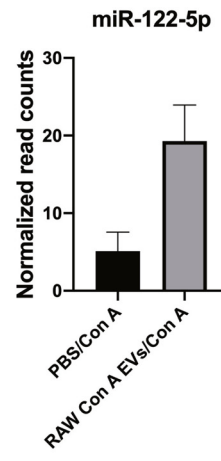
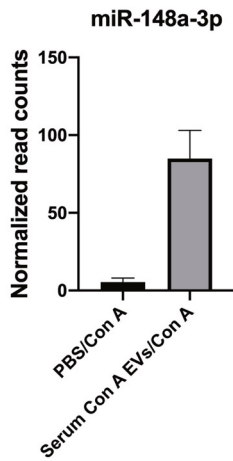
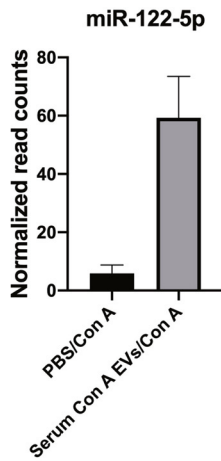
Upregulated miRNAs in RAW264.7

Upregulated miRNAs in EVs



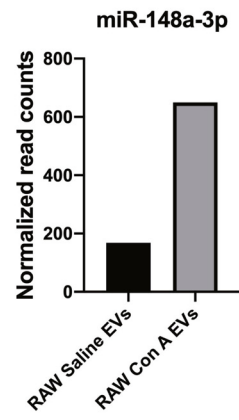
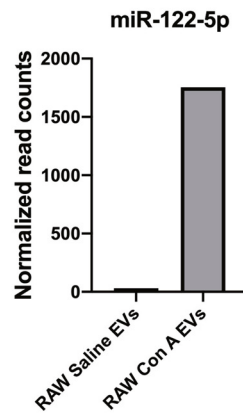
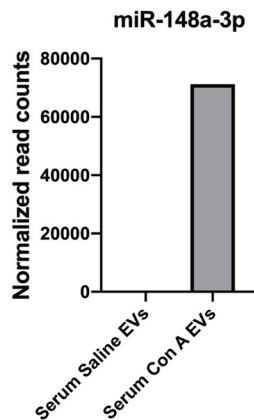
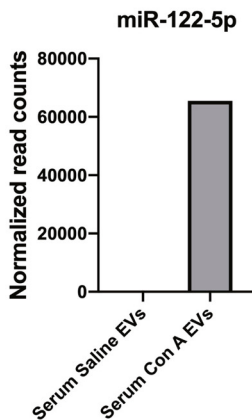
(B) Serum Con A EVs-treated RAW264.7

(C) RAW Con A EVs-treated RAW264.7



(D) Serum EVs

(E) RAW EVs



(caption on next page)

Fig. 6. Upregulation of *mmu-miR-122-5p* and *mmu-miR-148a-3p* expression in EVs from the serum of Con A-treated mice and from Con A-treated RAW264.7 cells and the EVs-treated cells.

miRNA-seq in EVs/Con A-cotreated RAW264.7 cells (n = 3/group) and EVs (n = 1/group) was performed, and Venn diagrams were generated. The number of upregulated miRNAs in Serum Con A EVs/Con A-cotreated RAW264.7 cells and RAW Con A EVs/Con A-cotreated cells compared with PBS/Con A-cotreated cells is shown (A, upper left panel). The number of upregulated miRNAs in Serum Con A EVs compared with Serum Saline EVs and RAW Con A EVs compared with RAW Saline EVs is shown (A, upper right panel). The number of each commonly upregulated miRNAs in the RAW264.7 samples or the EVs samples is shown (A, lower panel). In the RAW264.7 samples, upregulated miRNAs were identified with a q value < 0.1 and a fold change > 2. In the EVs samples, upregulated miRNAs were identified with a fold change > 2. The normalized read counts of *mmu-miR-122-5p* and *mmu-miR-148a-3p* in the Serum Con A EVs/Con A-cotreated RAW264.7 cells (B), the RAW Con A EVs/Con A-cotreated cells (C), the Serum EVs (D) and the RAW EVs (E) are shown. The data are shown as the mean value ± S.D.

Table 1

Top 30 enriched KEGG pathways of the predicted target genes of *mmu-miR-122-5p* and *mmu-miR-148a-3p*

Pathways	Count	%	p value
<i>mmu04150</i> : mTOR signaling pathway	18	30.51	1.22E-07
<i>mmu04910</i> : Insulin signaling pathway	27	19.29	1.02E-06
<i>mmu04919</i> : Thyroid hormone signaling pathway	21	18.42	4.30E-05
<i>mmu04068</i> : FoxO signaling pathway	23	17.16	5.19E-05
<i>mmu04722</i> : Neurotrophin signaling pathway	21	17.21	1.15E-04
<i>mmu04360</i> : Axon guidance	21	16.28	2.52E-04
<i>mmu05200</i> : Pathways in cancer	45	11.39	3.20E-04
<i>mmu04660</i> : T cell receptor signaling pathway	17	16.83	8.06E-04
<i>mmu05221</i> : Acute myeloid leukemia	12	21.43	8.59E-04
<i>mmu04510</i> : Focal adhesion	27	13.04	9.75E-04
<i>mmu04130</i> : SNARE interactions in vesicular transport	9	27.27	1.04E-03
<i>mmu05211</i> : Renal cell carcinoma	13	19.12	1.37E-03
<i>mmu05215</i> : Prostate cancer	15	17.05	1.61E-03
<i>mmu05220</i> : Chronic myeloid leukemia	13	18.06	2.28E-03
<i>mmu05212</i> : Pancreatic cancer	12	18.46	3.03E-03
<i>mmu05223</i> : Non-small cell lung cancer	11	19.64	3.09E-03
<i>mmu04350</i> : TGF-β signaling pathway	14	16.47	3.34E-03
<i>mmu05205</i> : Proteoglycans in cancer	25	12.32	3.40E-03
<i>mmu04931</i> : Insulin resistance	16	14.55	5.19E-03
<i>mmu05231</i> : Choline metabolism in cancer	15	14.85	5.89E-03
<i>mmu05213</i> : Endometrial cancer	10	19.23	6.07E-03
<i>mmu04810</i> : Regulation of actin cytoskeleton	25	11.74	6.26E-03
<i>mmu04010</i>: MAPK signaling pathway	28	11.16	7.19E-03
<i>mmu04917</i> : Prolactin signaling pathway	12	16.44	7.51E-03
<i>mmu04151</i>: PI3K-Akt signaling pathway	36	10.26	7.98E-03
<i>mmu05222</i> : Small cell lung cancer	13	15.48	8.21E-03
<i>mmu05230</i> : Central carbon metabolism in cancer	11	17.19	8.21E-03
<i>mmu04550</i> : Signaling pathways regulating pluripotency of stem cells	18	13.04	8.51E-03
<i>mmu05214</i> : Glioma	11	16.92	9.15E-03
<i>mmu04070</i> : Phosphatidylinositol signaling system	14	14.43	1.03E-02

The top 30 enriched KEGG pathways in the predicted target genes of *mmu-miR-122-5p* and *mmu-miR-148a-3p* are listed. The enriched pathways were identified using a p value < 0.05. "Count" indicates the number of predicted target genes in each pathway. "%" indicates the proportion of predicted target genes among the genes in each pathway.

3.7. Knockdown of the EVs secretion regulator *RAB27A* exacerbated Con A-induced hepatitis

To examine the involvement of EVs in Con A-induced hepatitis *in vivo*, *Rab27a*, a positive regulator of EVs secretion from cells (Ostrowski et al., 2010; Yang et al., 2018), RNA interference was performed in the model mice using AdV. A significant increase in *RAB27A* protein levels was observed in the livers 9 h after Con A administration. The increase was significantly suppressed in the AdV *Rab27a* shRNA (Rab sh)-cotreated group compared with the AdV scrambled shRNA (scr sh)-cotreated group (Fig. 8A). Contrary to our expectations, there was no difference in the serum EVs number between the AdV Rab sh/Con A-cotreated group and the AdV scr sh/Con A-cotreated group 9 h after Con A administration (Fig. 8B). However, the serum ALT level in the AdV Rab sh/Con A-cotreated group was significantly higher than that in the AdV scr sh/Con A-cotreated group 9 h after Con A administration (Fig. 8C).

4. Discussion

EVs regulate the development and progression of various types of liver failure through immunoregulation (Hirsova et al., 2016; Momen-Heravi et al., 2015; Yang et al., 2018). In this study, we investigated the immunoregulatory function of EVs in Con A-induced hepatitis, which is widely used as a relevant model of human autoimmune hepatitis (Xue et al., 2015).

The liver is composed of parenchymal cells, namely, hepatocytes, and nonparenchymal cells, such as Kupffer cells (Oda et al., 2018). Con A treatment significantly increased the number of EVs secreted by RAW264.7 cells, a macrophage cell line, but not Hepa1-6 cells, a hepatoma cell line (Figs. 2D and 2E). These data suggest that the increased serum EVs in the Con A-treated mice (Fig. 1E) are derived from macrophages, such as Kupffer cells, rather than hepatocytes.

In Con A-induced hepatitis, macrophages infiltrate the liver and play an important role in the induction of injury through inflammatory cytokine production (Xue et al., 2015; Zheng et al., 2016). *IL-6*, *IL-1β* and *TNF-α* mRNA expression levels were commonly increased in the livers of Con A-treated mice and Con A-treated RAW264.7 cells (Fig. 3). Macrophages are one of the sources of these inflammatory cytokines in the liver; therefore, macrophages are assumed to produce the cytokines in the liver of Con A-treated mice.

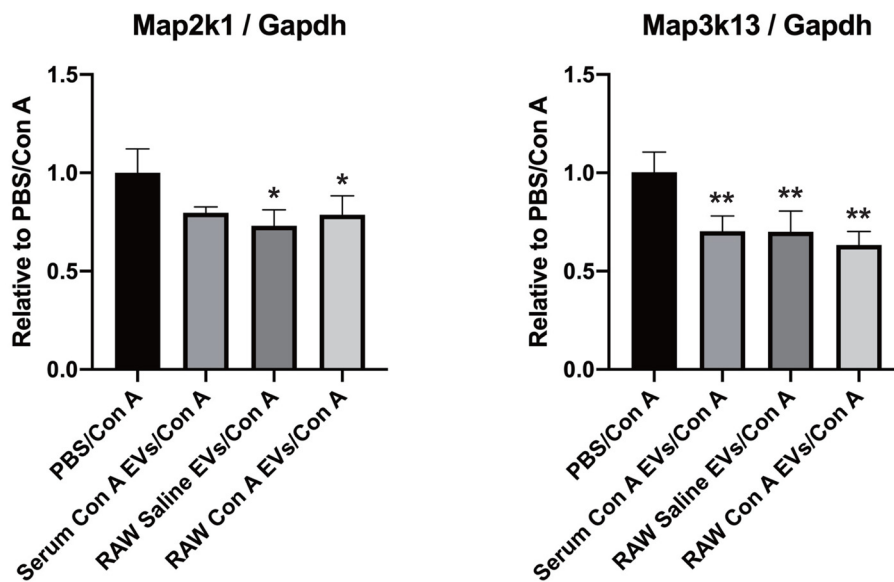
By intravenous injection, a large number of RAW264.7 cell-derived EVs can be distributed to the liver (Zheng et al., 2019), and various cell-derived EVs are taken up by hepatic macrophages (Imai et al., 2015; Tamura et al., 2016; Willekens et al., 2005); therefore, the increased serum EVs in the present study (Fig. 1E) are likely to be distributed to the liver and taken up by hepatic macrophages. Various cell-derived EVs have been reported to suppress the LPS-induced immune response in monocytes and macrophages (Holman et al., 2019; Shao et al., 2020; Zheng et al., 2019). Therefore, we examined the effects of EVs from this model mouse serum and Con A-treated RAW264.7 cells on inflammatory cytokine production in macrophage-derived cells. EVs pretreatment significantly suppressed inflammatory cytokine expression in Con A-stimulated RAW264.7 cells (Figs. 4C-4 F). EVs treatment did not suppress cell viability (Fig. 4B), suggesting that the suppression of inflammatory cytokine production is not due to cytotoxicity.

In the Con A-administered mice, the mean serum EVs number was greater than $8E + 09$ particles/mL at 3, 6 and 9 h after administration (Fig. 1E); therefore, the *in vivo* EVs exposure appears to exceed the *in vitro* EVs treatment concentration ($6E + 09$ particles/mL) from 3 h after administration (Fig. 1E). These data suggest that the phenomena observed in the *in vitro* study can be extrapolated to the *in vivo* model.

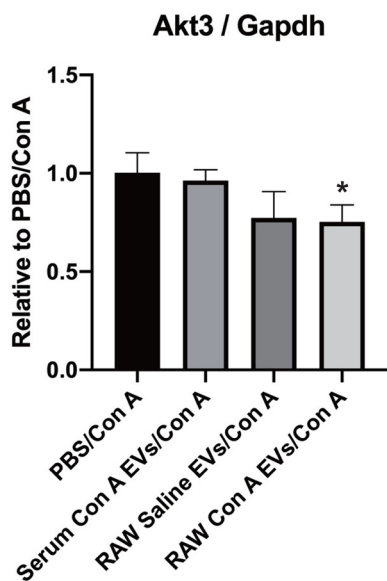
IL-6 plays both harmful and protective roles in Con A-induced hepatitis (Hong et al., 2002; Tagawa et al., 2000). *IL-6* mRNA expression level was most markedly suppressed among the evaluated cytokines in RAW Con A EVs and Serum Con A EVs-pretreated cells (Figs. 4C-4 F). These data suggest that macrophage-derived EVs may protect against Con A-induced hepatitis through the suppression of the production of inflammatory cytokines, such as *IL-6*.

In the miRNA-seq analysis, the expression of *mmu-miR-122-5p* and *mmu-miR-148a-3p* was significantly increased in the Serum Con A EVs, RAW Con A EVs and the EVs-treated cells (Fig. 6). *miR-122-5p* in hepatocyte-derived EVs is reported to enhance inflammatory cytokine production through the suppression of heme oxygenase-1 expression

(A) MAPK signaling pathway



(B) PI3K/Akt signaling pathway



(C) Rho/ROCK signaling pathway

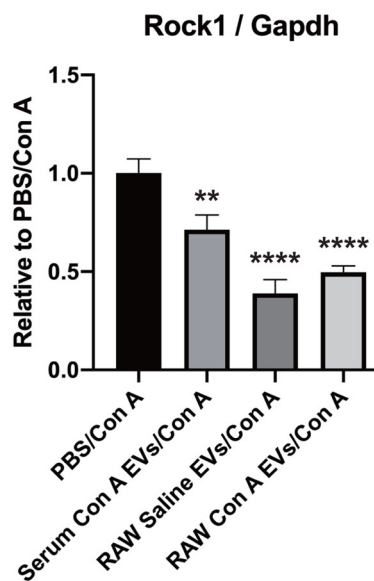


Fig. 7. Suppression of miRNA target gene expression in Con A-stimulated RAW264.7 cells by EVs pretreatment.

RAW264.7 cells were pretreated with $6E + 09$ particles/mL various EVs for 8 h, followed by 50 μ g/mL Con A treatment for 16 h. *Map2k1*, *Map3k13* (A), *Akt3* (B) and *Rock1* (C) mRNA levels in the cells were analyzed by qPCR (n = 3/group). The mRNA levels were normalized to those of *Gapdh*. The data are shown as the mean value \pm S.D. Differences in comparisons with the PBS/Con A-cotreated group were considered significant at *p < 0.05, **p < 0.01 and ****p < 0.0001.

Table 2

Predicted or validated mmu-miR-122-5p and mmu-miR-148a-3p target genes

Target genes	miRNAs	Number of algorithms in miRWalk2.0	miRTarbase
<i>Map2k1</i>	mmu-miR-148a-3p	8	-
<i>Map3k13</i>	mmu-miR-148a-3p	8	-
<i>Akt3</i>	mmu-miR-122-5p	8	-
<i>Rock1</i>	mmu-miR-148a-3p	8	Validated

(Momen-Heravi et al., 2015; Zhao et al., 2020), which is the opposite tendency found in the present study. On the other hand, miR-148a-3p is reported to suppress inflammatory gene expression through the suppression of nuclear factor-kappa B (NF- κ B) and MAPK pathways in human aortic valve interstitial cells and Huh-7.5.1 cells, respectively (Deng et al., 2019; Patel et al., 2015). Our data suggest that these miRNAs are involved in the immunoregulation observed in EVs-treated cells.

The expression of inflammatory cytokines such as IL-6 is regulated by the NF- κ B pathway and MAPK pathways: extracellular signal-regulated kinases (ERK), c-Jun-N-terminal kinase (JNK) and p38 pathways (Deng et al., 2019; Hou et al., 2018; Zhuang et al., 2016). In addition,

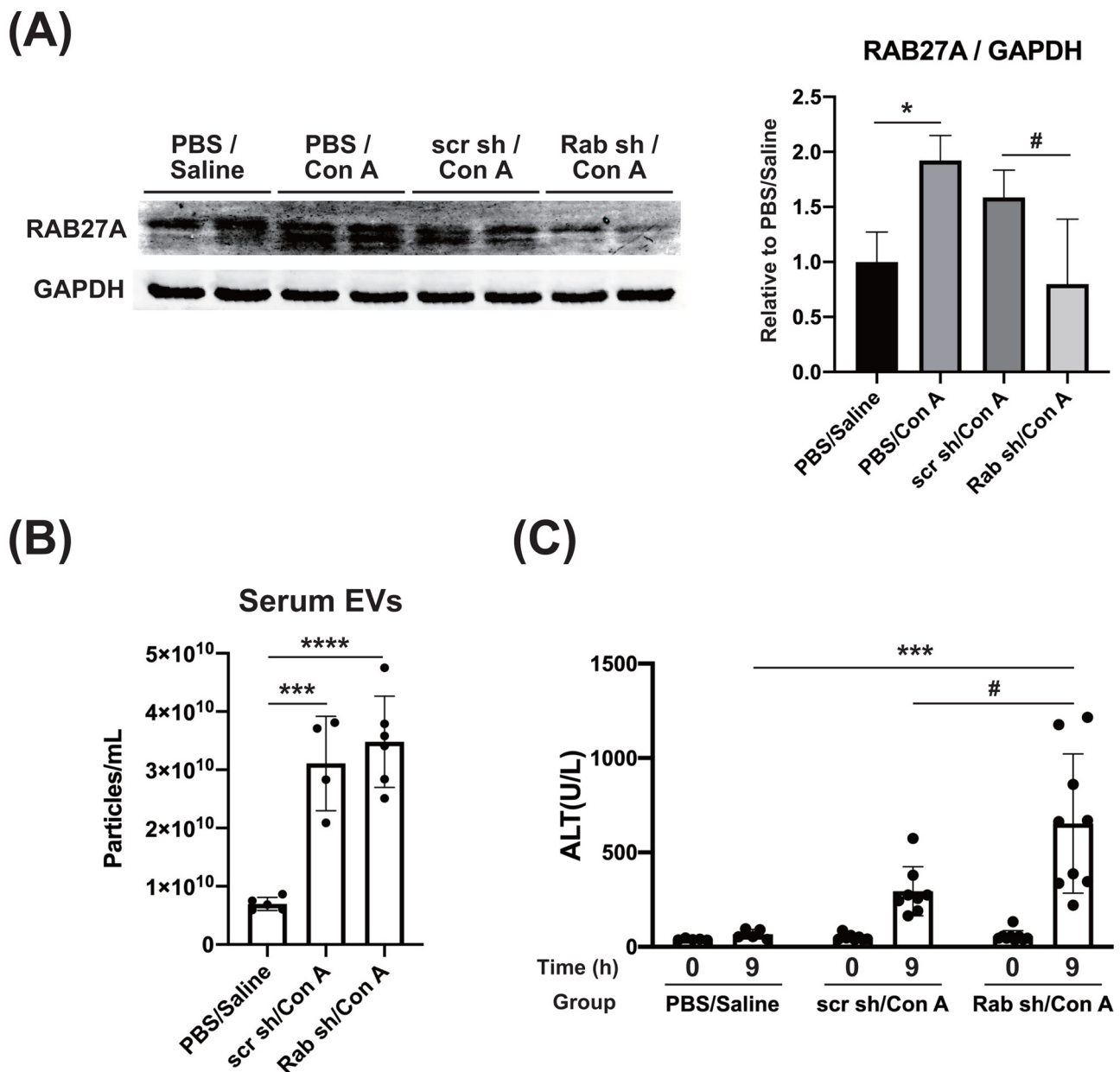


Fig. 8. Exacerbation of Con A-induced hepatitis by RAB27A knockdown.

Three days after the intravenous administration of AdV *mRab27a* shRNA (Rab sh) or AdV scrambled shRNA (scr sh), the mice were administered Con A. Liver RAB27A protein levels were analyzed 9 h after the administration of Con A by Western blotting. GAPDH was used as a loading control. Representative blot images and the RAB27A levels relative to those of the PBS/Saline-coadministered group are shown ($n = 4$ /group) (A). The serum EVs numbers 9 h after administration of Con A are shown ($n = 4-6$) (B). The serum ALT levels just before or 9 h after the administration of Con A are shown ($n = 5-9$) (C). The data are shown as the mean value \pm S.D. Differences in comparisons with the PBS/Saline-coadministered group were considered significant at * $p < 0.05$, *** $p < 0.001$ and **** $p < 0.0001$. Differences in comparisons with the scr sh/Con A-coadministered group were considered significant at # $p < 0.05$.

the PI3K/Akt pathway (Li et al., 2019; Vergadi et al., 2017) and Rho/ROCK pathway regulate these pathways (Cheng et al., 2015). The expression of the mmu-miR-122-5p and mmu-miR-148a-3p target genes in these pathways (MAPK pathway, PI3K/Akt pathway and Rho/ROCK pathway) was suppressed by EVs treatment (Fig. 7). MAP2K1 activates the ERK pathway through the phosphorylation of ERK1/2 (Hou et al., 2018). MAP3K13, also known as leucine zipper-bearing kinase, activates the JNK and NF- κ B pathways (Ikeda et al., 2001; Masaki et al., 2003). The Akt family in the PI3K/Akt pathway consists of three isoforms: AKT1, AKT2 and AKT3. Li et al. reported that AKT3 knockdown inhibits the JNK and NF- κ B pathways and suppresses inflammatory cytokine expression in LPS-treated A549 cells (Li et al., 2019). ROCK, a serine/threonine kinase, is the first downstream effector of RhoA. ROCK

enhances inflammatory cytokine production through the activation of the JNK and ERK pathways in RAW264.7 cells (Cheng et al., 2015). Taking these reported data into account, in the present study, we suggest that miR-122-5p and miR-148a-3p may suppress inflammatory cytokine production by suppressing the expression of the target genes in these pathways.

In the present *in vitro* EVs treatment study in which all groups were treated with the same number of EVs, pretreatment with RAW Saline EVs, as well as RAW Con A EVs, suppressed the mRNA expression of *IL-6* and the miRNA target genes in RAW264.7 cells (Figs. 4C and 7). In addition, the two groups showed similar miRNA profiles by cluster analysis (Fig. 5A), indicating that miRNA profiles per EV particle are similar between the two groups. However, the secreted EVs number in

the culture supernatant of Con A-treated RAW264.7 cells was significantly increased (Fig. 2D). In the present study, the EVs miRNAs analysis was performed by the normalization method using a spike-in control; therefore, the analysis results likely account for the difference in the EVs number between samples. In the EVs miRNAs analysis, the normalized counts of miR-122-5p and miR-148a-3p in RAW Con A EVs were much higher than those in RAW Saline EVs (Fig. 6E), suggesting that changes in the EVs number rather than in the EVs cargo may play an important role in Con A-induced hepatitis.

Although we focused on miRNAs and target genes as the EVs immunoregulatory factors in the present study, previous studies showed that EVs regulate various diseases by transporting ligand proteins (Hirsova et al., 2016), long noncoding RNAs (Takahashi et al., 2014) and oxidized phospholipids (Yang et al., 2018) between cells. Thus, various types of molecules other than miRNAs may also be involved in the hepatitis. The Serum Con A EVs-treated cells, in which the miR-122-5p and miR-148a-3p read counts were much higher than those in the RAW Con A EVs-treated cells (Figs. 6B and 6C), showed more potent suppression of inflammatory cytokine production than the RAW Con A EVs-treated cells (Figs. 4C–4F). However, there was no difference in the degree of suppression of the target gene expression between the groups (Fig. 7), suggesting that other factors are also involved in this phenomenon. Further studies will be needed in the future.

In the present *in vitro* study, we analyzed using a macrophage cell line, RAW264.7 cells. Further studies using primary cells, hepatic macrophages, will also be needed in the future.

Hepatic RAB27A knockdown exacerbated the Con A-induced hepatitis (Fig. 8C). RAB27A protein, a small GTPase, promotes EVs secretion from cells through the regulation of multivesicular endosome docking at the plasma membrane (Ostrowski et al., 2010). Hepatic RAB27A regulates EVs secretion in hepatic ischemia/reperfusion injury (Yang et al., 2018), and EVs secretion is suppressed in bone marrow-derived macrophages from RAB27A-deficient mice (Smith et al., 2017). Since AdV mainly accumulates in the liver and infects hepatocytes and hepatic macrophages after intravenous administration (Wheeler et al., 2001), we assumed that hepatic macrophage RAB27A was knocked down in the present experiment. The suppression of EVs production in hepatic macrophages may have caused the exacerbation of hepatitis.

We evaluated the effect of RAB27A knockdown on IL-6 levels in Con A-administered mice. However, the IL-6 protein levels in the serum and the IL-6 mRNA levels in the whole liver tissues of the mice 9 hours after the Con A administration were not affected by RAB27A knockdown (data not shown). Further *in vivo* study are needed to make the EVs immunoregulatory function clearer.

Contrary to our expectation, hepatic RAB27A knockdown did not reduce the serum EVs numbers in the model mice (Fig. 8B). It appears that the source of the increased serum EVs in Con A-administered mice is not only hepatic macrophages because Con A administration to mice causes tissue damage and macrophage infiltration in the spleen and kidney as well as the liver (Liu et al., 2015; Yang et al., 2019). This may be a reason why RAB27A knockdown using AdV, which mainly accumulates in the liver, did not reduce the serum EVs number.

While RAB27A protein is a known EVs secretion regulator, RAB27A also positively regulates cytotoxic granule exocytosis in cytotoxic T-lymphocytes, natural killer cells and neutrophils. Due to disorder of the function, *Rab27a* mutants cause severe immunodeficiency known as Griscelli syndrome (Menasche et al., 2003). In the present study, Con A-induced hepatitis was exacerbated but not attenuated by RAB27A knockdown (Fig. 8C), suggesting that this phenomenon is dependent on EVs release regulation rather than granule exocytosis regulation.

In summary, we found that macrophage-derived EVs suppress cytokine expression in macrophages by transporting miRNAs and regulate Con A-induced hepatitis. EVs treatment or the improvement of EVs secretion might be a therapeutic strategy for immune-mediated hepatitis.

Funding

This study was supported by a Grant-in-Aid for Scientific Research (B) (No. 19H03388) from the Japan Society for the Promotion of Science.

Declaration of Competing Interest

The authors declare that they have no known competing financial interests or personal relationships that could have appeared to influence the work reported in this paper.

Acknowledgements

We would like to thank Dr. Yusuke Yoshioka and Dr. Takahiro Ochiya in the Division of Molecular and Cellular Medicine at the Institute of Medical Science Tokyo Medical University for their assistance with the EVs isolation.

Appendix A. Supplementary data

Supplementary material related to this article can be found, in the online version, at doi:<https://doi.org/10.1016/j.tox.2020.152544>.

References

- Alexander, M., Ramstead, A.G., Bauer, K.M., Lee, S.H., Runtsch, M.C., Wallace, J., Huffaker, T.B., Larsen, D.K., Tolmacheva, T., Seabra, M.C., Round, J.L., Ward, D.M., O'Connell, R.M., 2017. Rab27-dependent exosome production inhibits chronic inflammation and enables acute responses to inflammatory stimuli. *J. Immunol.* 199, 3559–3570.
- Cheng, C.I., Chen, P.H., Lin, Y.C., Kao, Y.H., 2015. High glucose activates Raw264.7 macrophages through RhoA kinase-mediated signaling pathway. *Cell Signal* 27, 283–292.
- Deng, Y., Wang, J., Huang, M., Xu, G., Wei, W., Qin, H., 2019. Inhibition of miR-148a-3p resists hepatocellular carcinoma progress of hepatitis C virus infection through suppressing c-Jun and MAPK pathway. *J. Cell Mol. Med.* 23, 1415–1426.
- Dweep, H., Gretz, N., 2015. miRWalk 2.0: a comprehensive atlas of microRNA-target interactions. *Nat. Methods* 12, 697.
- Gong, J., Guan, L., Tian, P., Li, C., Zhang, Y., 2018. Rho kinase type 1 (ROCK1) promotes lipopolysaccharide-induced inflammation in corneal epithelial cells by activating toll-like receptor 4 (TLR4)-mediated signaling. *Med. Sci. Monit.* 24, 3514–3523.
- Harrill, A.H., McCullough, S.D., Wood, C.E., Kahle, J.J., Chorley, B.N., 2016. MicroRNA biomarkers of toxicity in biological matrices. *Toxicol. Sci.* 152, 264–272.
- Hirsova, P., Ibrahim, S.H., Krishnan, A., Verma, V.K., Bronk, S.F., Werneburg, N.W., Charlton, M.R., Shah, V.H., Malhi, H., Gores, G.J., 2016. Lipid-induced signaling causes release of inflammatory extracellular vesicles from hepatocytes. *Gastroenterology* 150, 956–967.
- Holman, N.S., Church, R.J., Nautiyal, M., Rose, K.A., Thacker, S.E., Otieno, M.A., Wolf, K.K., LeCluyse, E., Watkins, P.B., Mosedale, M., 2019. Hepatocyte-derived exosomes promote liver immune tolerance: possible implications for idiosyncratic drug-induced liver injury. *Toxicol. Sci.* 170, 499–508.
- Hong, F., Jaruga, B., Kim, W.H., Radaeva, S., El-Assal, O.N., Tian, Z., Nguyen, V.A., Gao, B., 2002. Opposing roles of STAT1 and STAT3 in T cell-mediated hepatitis: regulation by SOCS. *J. Clin. Invest.* 110, 1503–1513.
- Hou, R., Han, Y., Fei, Q., Gao, Y., Qi, R., Cai, R., Qi, Y., 2018. Dietary flavone tectochrysin exerts anti-inflammatory action by directly inhibiting MEK1/2 in LPS-primed macrophages. *Mol. Nutr. Food Res.* 62.
- Huang, d.W., Sherman, B.T., Lempicki, R.A., 2009. Bioinformatics enrichment tools: paths toward the comprehensive functional analysis of large gene lists. *Nucleic Acids Res.* 37, 1–13.
- Huang, H.Y., Lin, Y.C., Li, J., Huang, K.Y., Shrestha, S., Hong, H.C., Tang, Y., Chen, Y.G., Jin, C.N., Yu, Y., Xu, J.T., Li, Y.M., Cai, X.X., Zhou, Z.Y., Chen, X.H., Pei, Y.Y., Hu, L., Su, J.J., Cui, S.D., Wang, F., Xie, Y.Y., Ding, S.Y., Luo, M.F., Chou, C.H., Chang, N.W., Chen, K.W., Cheng, Y.H., Wan, X.H., Hsu, W.L., Lee, T.Y., Wei, F.X., Huang, H.D., 2020. miRTarBase 2020: updates to the experimentally validated microRNA-target interaction database. *Nucleic Acids Res.* 48, D148–D154.
- Ikeda, A., Hasegawa, K., Masaki, M., Moriguchi, T., Nishida, E., Kozutsumi, Y., Oka, S., Kawasaki, T., 2001. Mixed lineage kinase LZK forms a functional signaling complex with JIP-1, a scaffold protein of the c-Jun NH(2)-terminal kinase pathway. *J. Biochem.* 130, 773–781.
- Imai, T., Takahashi, Y., Nishikawa, M., Kato, K., Morishita, M., Yamashita, T., Matsumoto, A., Charoenviriyakul, C., Takakura, Y., 2015. Macrophage-dependent clearance of systemically administered B16BL6-derived exosomes from the blood circulation in mice. *J. Extracell. Vesicles* 4, 26238.
- Laemmli, U.K., 1970. Cleavage of structural proteins during the assembly of the head of bacteriophage T4. *Nature* 227, 680–685.

- Lawrie, C.H., Gal, S., Dunlop, H.M., Pushkaran, B., Liggins, A.P., Pulford, K., Banham, A.H., Pezzella, F., Boultonwood, J., Wainscoat, J.S., Hatton, C.S., Harris, A.L., 2008. Detection of elevated levels of tumour-associated microRNAs in serum of patients with diffuse large B-cell lymphoma. *Br. J. Haematol.* 141, 672–675.
- Li, P., Yao, Y., Ma, Y., Chen, Y., 2019. MiR-150 attenuates LPS-induced acute lung injury via targeting AKT3. *Int. Immunopharmacol.* 75, 105794.
- Liu, C., Cheng, Z., Wang, Y., Dai, X., Zhang, J., Xue, D., 2015. Paeoniflorin exerts a nephroprotective effect on concanavalin A-induced damage through inhibition of macrophage infiltration. *Diagn. Pathol.* 10, 120.
- Marukawa, Y., Nakamoto, Y., Kakinoki, K., Tsuchiyama, T., Iida, N., Kagaya, T., Sakai, Y., Naito, M., Mukaida, N., Kaneko, S., 2012. Membrane-bound form of monocyte chemoattractant protein-1 enhances antitumor effects of suicide gene therapy in a model of hepatocellular carcinoma. *Cancer Gene Ther.* 19, 312–319.
- Masaki, M., Ikeda, A., Shiraki, E., Oka, S., Kawasaki, T., 2003. Mixed lineage kinase LZK and antioxidant protein-1 activate NF-kappaB synergistically. *Eur. J. Biochem.* 270, 76–83.
- McDonald, M.K., Tian, Y., Qureshi, R.A., Gormley, M., Ertel, A., Gao, R., Aradillas Lopez, E., Alexander, G.M., Sacan, A., Fortina, P., Ajit, S.K., 2014. Functional significance of macrophage-derived exosomes in inflammation and pain. *Pain* 155, 1527–1539.
- Menasche, G., Feldmann, J., Houdusse, A., Desaymard, C., Fischer, A., Goud, B., de Saint Basile, G., 2003. Biochemical and functional characterization of Rab27a mutations occurring in Griscelli syndrome patients. *Blood* 101, 2736–2742.
- Momen-Heravi, F., Bala, S., Kodys, K., Szabo, G., 2015. Exosomes derived from alcohol-treated hepatocytes horizontally transfer liver specific miRNA-122 and sensitize monocytes to LPS. *Sci. Rep.* 5, 9991.
- Oda, S., Takeuchi, M., Akai, S., Shirai, Y., Tsuneyama, K., Yokoi, T., 2018. miRNA in rat liver sinusoidal endothelial cells and hepatocytes and application to circulating biomarkers that discern pathogenesis of liver injuries. *Am. J. Pathol.* 188, 916–928.
- Ostrowski, M., Carmo, N.B., Krumeich, S., Fangeit, I., Raposo, G., Savina, A., Moita, C.F., Schauer, K., Hume, A.N., Freitas, R.P., Goud, B., Benaroch, P., Hacohen, N., Fukuda, M., Desnos, C., Seabra, M.C., Darchen, F., Amigorena, S., Moita, L.F., Thery, C., 2010. Rab27a and Rab27b control different steps of the exosome secretion pathway. *Nat. Cell Biol.* 12 (19–30), 11–13.
- Patel, V., Carrion, K., Hollands, A., Hinton, A., Gallegos, T., Dyo, J., Sasik, R., Leire, E., Hardiman, G., Mohamed, S.A., Nigam, S., King, C.C., Nizet, V., Nigam, V., 2015. The stretch responsive microRNA miR-148a-3p is a novel repressor of IKK β , NF- κ B signaling, and inflammatory gene expression in human aortic valve cells. *FASEB J.* 29, 1859–1868.
- Saha, B., Momen-Heravi, F., Kodys, K., Szabo, G., 2016. MicroRNA cargo of extracellular vesicles from alcohol-exposed monocytes signals naive monocytes to differentiate into M2 macrophages. *J. Biol. Chem.* 291, 149–159.
- Seo, W., Eun, H.S., Kim, S.Y., Yi, H.S., Lee, Y.S., Park, S.H., Jang, M.J., Jo, E., Kim, S.C., Han, Y.M., Park, K.G., Jeong, W.I., 2016. Exosome-mediated activation of toll-like receptor 3 in stellate cells stimulates interleukin-17 production by $\gamma\delta$ T cells in liver fibrosis. *Hepatology* 64, 616–631.
- Shao, M., Xu, Q., Wu, Z., Chen, Y., Shu, Y., Cao, X., Chen, M., Zhang, B., Zhou, Y., Yao, R., Shi, Y., Bu, H., 2020. Exosomes derived from human umbilical cord mesenchymal stem cells ameliorate IL-6-induced acute liver injury through miR-455-3p. *Stem Cell Res. Ther.* 11, 37.
- Smith, V.L., Cheng, Y., Bryant, B.R., Schorey, J.S., 2017. Exosomes function in antigen presentation during an in vivo Mycobacterium tuberculosis infection. *Sci. Rep.* 7, 43578.
- Stravitz, R.T., Lee, W.M., 2019. Acute liver failure. *Lancet* 394, 869–881.
- Su, W., Sun, J., Shimizu, K., Kadota, K., 2019. TCC-GUI: a Shiny-based application for differential expression analysis of RNA-Seq count data. *BMC Res. Notes* 12, 133.
- Tagawa, Y., Matthys, P., Heremans, H., Dillen, C., Zaman, Z., Iwakura, Y., Billiau, A., 2000. Bimodal role of endogenous interleukin-6 in concanavalin A-induced hepatitis in mice. *J. Leukoc. Biol.* 67, 90–96.
- Takahashi, K., Yan, I.K., Wood, J., Haga, H., Patel, T., 2014. Involvement of extracellular vesicle long noncoding RNA (linc-VLDLR) in tumor cell responses to chemotherapy. *Mol. Cancer Res.* 12, 1377–1387.
- Tamura, R., Uemoto, S., Tabata, Y., 2016. Immunosuppressive effect of mesenchymal stem cell-derived exosomes on a concanavalin A-induced liver injury model. *Inflamm. Regen.* 36, 26.
- Taylor, D.D., Gerceel-Taylor, C., 2013. The origin, function, and diagnostic potential of RNA within extracellular vesicles present in human biological fluids. *Front. Genet.* 4, 142.
- Tominaga, N., Kosaka, N., Ono, M., Katsuda, T., Yoshioka, Y., Tamura, K., Lötvall, J., Nakagama, H., Ochiya, T., 2015. Brain metastatic cancer cells release microRNA-181c-containing extracellular vesicles capable of destructing blood-brain barrier. *Nat. Commun.* 6, 6716.
- Ugai, H., Yamasaki, T., Hirose, M., Inabe, K., Kujime, Y., Terashima, M., Liu, B., Tang, H., Zhao, M., Murata, T., Kimura, M., Pan, J., Obata, Y., Hamada, H., Yokoyama, K.K., 2005. Purification of infectious adenovirus in two hours by ultracentrifugation and tangential flow filtration. *Biochem. Biophys. Res. Commun.* 331, 1053–1060.
- Vergadi, E., Ieronymaki, E., Lyroni, K., Vaporidi, K., Tsatsanis, C., 2017. Akt signaling pathway in macrophage activation and M1/M2 polarization. *J. Immunol.* 198, 1006–1014.
- Wheeler, M.D., Yamashina, S., Froh, M., Rusyn, I., Thurman, R.G., 2001. Adenoviral gene delivery can inactivate Kupffer cells: role of oxidants in NF-kappaB activation and cytokine production. *J. Leukoc. Biol.* 69, 622–630.
- Willekens, F.L., Werre, J.M., Kruijt, J.K., Roerdinkholder-Stoelwinder, B., Groenen-Döpp, Y.A., van den Bos, A.G., Bosman, G.J., van Berkel, T.J., 2005. Liver Kupffer cells rapidly remove red blood cell-derived vesicles from the circulation by scavenger receptors. *Blood* 105, 2141–2145.
- Xue, J., Chen, F., Wang, J., Wu, S., Zheng, M., Zhu, H., Liu, Y., He, J., Chen, Z., 2015. Emodin protects against concanavalin A-induced hepatitis in mice through inhibiting activation of the p38 MAPK-NF- κ B signaling pathway. *Cell Physiol. Biochem.* 35, 1557–1570.
- Yang, J., Wang, B., Zhang, C.F., Xu, X.H., Zhang, M., 2019. A C₂₁-steroidal glycoside from *Cynanchum atratum* attenuates concanavalin A-induced liver injury in mice. *Molecules* 24, 1087.
- Yang, M.Q., Du, Q., Goswami, J., Varley, P.R., Chen, B., Wang, R.H., Morelli, A.E., Stolz, D.B., Billiar, T.R., Li, J., Geller, D.A., 2018. Interferon regulatory factor 1-Rab27a regulated extracellular vesicles promote liver ischemia/reperfusion injury. *Hepatology* 67, 1056–1070.
- Zhao, Z., Zhong, L., Li, P., He, K., Qiu, C., Zhao, L., Gong, J., 2020. Cholesterol impairs hepatocyte lysosomal function causing M1 polarization of macrophages via exosomal miR-122-5p. *Exp. Cell Res.* 387, 111738.
- Zheng, W., Wang, Q., Lu, X., Shi, Q., Zou, J., Tao, Y., Wang, P., 2016. Protective effects of *Dracocephalum heterophyllum* in conA-induced acute hepatitis. *Mediators Inflamm.* 2016, 2684321.
- Zheng, Y., He, R., Wang, P., Shi, Y., Zhao, L., Liang, J., 2019. Exosomes from LPS-stimulated macrophages induce neuroprotection and functional improvement after ischemic stroke by modulating microglial polarization. *Biomater. Sci.* 7, 2037–2049.
- Zhuang, Y., Li, Y., Li, X., Xie, Q., Wu, M., 2016. Atg7 knockdown augments concanavalin A-induced acute hepatitis through an ROS-mediated p38/MAPK pathway. *PLoS One* 11, e0149754.